RESEARCH ARTICLE

Key Points:
- Most aspen stands in Utah cannot survive on growing season rain and local soil moisture as their only water supply
- Aspen stands in Utah are highly dependent on a groundwater subsidy and vulnerable to any subsidy shortfall
- Aspen stand health in Utah will be threatened by diminished winter snowpack

Correspondence to:
D. M. Love,
david.love@uga.edu

Dependence of Aspen Stands on a Subsurface Water Subsidy: Implications for Climate Change Impacts

D. M. Love[1,2] [ID], M. D. Venturas[1] [ID], J. S. Sperry[1] [ID], P. D. Brooks[3] [ID], J. L. Pettit[4], Y. Wang[1] [ID], W. R. L. Anderegg[1], X. Tai[5,3] [ID], and D. S. Mackay[5] [ID]

[1]School of Biological Sciences, University of Utah, Salt Lake City, UT, USA, [2]Now at Warnell School of Forestry and Natural Resources, University of Georgia, Athens, GA, USA, [3]Department of Geology and Geophysics, University of Utah, Salt Lake City, UT, USA, [4]Department of Wildland Resources, Utah State University, Logan, UT, USA, [5]Department of Geography, State University of New York at Buffalo, Buffalo, NY, USA

Abstract The reliance of 10 Utah (USA) aspen forests on direct infiltration of growing season rain versus an additional subsurface water subsidy was determined from a trait- and process-based model of stomatal control. The model simulated the relationship between water supply to the root zone versus canopy transpiration and assimilation over a growing season. Canopy flux thresholds were identified that distinguished nonstressed, stressed, and dying stands. We found growing season rain and local soil moisture were insufficient for the survival of 5 of 10 stands. Six stands required a substantial subsidy (31–80% of potential seasonal transpiration) to avoid water stress and maximize photosynthetic potential. Subsidy dependence increased with stand hydraulic conductance. Four of the six "subsidized" stands were predicted to be stressed during the survey year owing to a subsidy shortfall. Since winter snowpack is closely related to groundwater recharge in the region, we compared winter precipitation with tree-ring chronologies. Consistent with model predictions, chronologies were more sensitive to snowpack in subsidized stands than in nonsubsidized ones. The results imply that aspen stand health in the region is more coupled to winter snowpack than to growing season water supply. Winters are predicted to have less precipitation as snow, indicating a stressful future for the region's aspen forests.

1. Introduction

Climate change is expected to increase the frequency and severity of drought for many regions (Dai, 2013), leading to predictions of significant tree mortality and reduced forest productivity over the coming century (Allen et al., 2010). Which forests will be most likely to succumb to drought? The answer involves a complex interplay between climatic change, hydrological processes mediating plant water supply, the physiological demand for water by the forest, and the limits to tree productivity and survival (McDowell et al., 2008; Powell et al., 2013; Sperry et al., 2016; Tai et al., 2017). Insights from plant hydraulics can inform the plant side of the story. A number of studies have found drought mortality to be associated with losses of plant hydraulic conductance of 60–90% (e.g., Adams et al., 2017; Brodribb & Cochard, 2009; Litvak et al., 2012; Rodríguez-Calcerrada et al., 2017; Venturas et al., 2016). The loss of plant hydraulic conductance from xylem cavitation and rhizosphere drying can be modeled from species' specific vulnerability curves and soil hydraulic properties (Mackay et al., 2015; McDowell et al., 2013; Sperry et al., 1998; Sperry et al., 2002; Sperry & Love, 2015; Sperry & Tyree, 1988). The canopy's demand for water can be predicted from an optimization of transpiration-induced loss of conductance versus concomitant carbon gain (Anderegg et al., 2018; Sperry et al., 2017; Wolf et al., 2016). Models that integrate these pieces (Sperry et al., 2017; Tai et al., 2018; Venturas et al., 2018) can be used to predict critical levels of root-zone water content that would reduce forest productivity and threaten their survival. The predictions of such models are backed by traits and process, which arguably makes them more appropriate forecasters than empirical models based on post hoc fitted parameters that have no physical or physiological meaning (Venturas et al., 2018).

Considering forest drought stress from a hydrological perspective, it is crucial to understand how water available for plants during the growing season is influenced by climate, topography, substrate, and rooting depth. The net amount of water withdrawn from soil by roots in a growing season ($\sum_s E$) potentially comes from three sources (Figure 1):
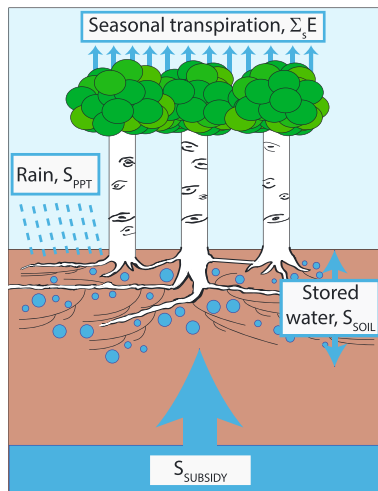
Figure 1. Conceptual diagram illustrating water sources for aspen stand seasonal transpiration ($\sum_s E$) and their representation in the one-dimensional soil-plant-atmosphere model. "Stored water, S_{SOIL}" represents water initially present in the soil column (assumed to be field capacity). "Rain, S_{PPT}" is the measured rainfall during the growing season, which was assumed to infiltrate soil to field capacity from the top down. "$S_{SUBSIDY}$" represents additional water from subsurface flow. For convenience this was modeled as vertical rise from a water table beneath the root zone as pictured.

$$\sum_s E = S_{SOIL} + S_{PPT} + S_{SUBSIDY}. \tag{1}$$

The S_{SOIL} is water from the drawdown in local soil water content of the root zone from its initial value at the beginning of growing season, S_{PPT} is water from precipitation on the stand during the growing season, and $S_{SUBSIDY}$ is water from any extra source. In a natural setting $S_{SUBSIDY}$ represents the potential contribution from groundwater, either through capillary rise or through lateral redistribution (Figure 1). The availability of the S_{SOIL} and S_{PPT} sources in equation (1) are relatively easy to quantify from growing season weather, substrate type, and rooting depth. The availability of the $S_{SUBSIDY}$ source is more difficult to predict, even where it defines the ecosystem as in riparian communities and wetlands (Tai et al., 2018). Although difficult to model, the influence of groundwater subsidy has emerged as an important process in predicting plant productivity and survival in many settings (Fan, 2015; Richter & Billings, 2015; Swetnam et al., 2017; Thompson et al., 2011). Hydrologic redistribution creates locally wet versus dry areas (Tai et al., 2017; Tai et al., 2018) and can buffer plants during dry seasons by delivering a subsidy to the root zone (Fan et al., 2017; Miguez-Macho & Fan, 2012; Naumburg et al., 2005; Newman et al., 2006). The presence of an additional water supply may promote the survival of species in hydrologic refugia during regional drought (Keppel et al., 2012; McLaughlin et al., 2017; Stewart et al., 2010). The dependence of a forest or species on a groundwater subsidy can substantially influence its response to climate change (Fan, 2015; Hanson & Weltzin, 2000; Swetnam et al., 2017).

This paper combines plant hydraulics with hydrology to assess the vulnerability to drought of aspen stands (*Populus tremuloides*) in Utah (USA) by determining the dependence of stand $\sum_s E$ and seasonal photosynthesis ($\sum_s A$, a proxy for productivity) on the $S_{SUBSIDY}$ term (equation (1)). Aspen is an important component of the montane forests of the intermountain west of the USA. In this snow-dominated environment, aspen's growing season is out of phase with the bulk of annual precipitation that comes in the winter as snow (Barnett et al., 2008; Castle et al., 2014). Groundwater recharged during snowmelt could continue to feed the aspen root zone during the much drier summer months (Maurer & Bowling, 2014). Winters in the intermountain west are expected to remain similarly wet over the coming century (Cayan et al., 2013), but with less precipitation as snow and more falling as rain (Barnett et al., 2008), which is less effective in recharging groundwater (Castle et al., 2014; Garreaud et al., 2017; Udall, 2013). Aspen in the neighboring state of Colorado has recently experienced significant drought-related mortality associated with cavitation-induced losses of plant hydraulic conductance (Anderegg et al., 2012; Anderegg et al., 2013). The spatial distribution of aspen mortality is generally consistent with topographically mediated redistribution of precipitation (Tai et al., 2017). Smaller snowpacks could reduce the amount of subsidy available to plants during the growing season (Figure 1), potentially stressing aspen forests. To the extent that aspen stands in the area depend on a subsidy, they may be more vulnerable to the loss of winter snowpack than to summer drought.

To assess aspen's dependency on groundwater subsidy, we modeled the relationship between root zone water supply and canopy function in terms of cumulative water demand ($\sum_s E$), cumulative canopy assimilation ($\sum_s A$), and mortality risk over a full growing season at 10 aspen stands across the state of Utah, USA. Aspen is amenable to modeling because of the homogenizing effect of its interconnected clonal growth and tendency to occur in mono-specific stands with limited understory. We used the carbon-gain versus hydraulic risk model of Sperry et al. (2017) as developed and tested for aspen by Venturas et al. (2018) in a research garden setting. This model assumes that plant gas exchange maximizes the difference between photosynthetic gain and hydraulic risk, where risk is the proximity to complete failure of water transport and canopy desiccation. The gain-risk model was found to represent aspen's observed drought response equally well as an empirical model that was fitted to the data (Venturas et al., 2018). The advantage of the gain-risk model is that all of its parameters are traits that can be measured or estimated (along with their uncertainties) a priori, making its predictions defensible under any combination of future environmental

conditions. The Venturas et al. (2018) study also established a mortality threshold for aspen: All trees that died from drought in their experiment were predicted by the model to exceed 85% loss of soil-to-leaf hydraulic conductance (PLC) by the end of the growing season.

To predict each stand's $S_{SUBSIDY}$ (equation (1)), we first zeroed out this term and modeled $\sum_s E$ assuming trees only had access to S_{SOIL} and S_{PPT} (soil starting at field capacity plus the rain incident on the stand during the growing season). This yielded $\sum_s E_{rain}$: the cumulative water use supplied by the S_{SOIL} and S_{PPT} water sources. We then added a water table beneath the root zone at different depths so that additional water could move to the root zone through capillary rise. Increasing water input in this manner allowed us to determine the maximum seasonal water use ($\sum_s E_{pot}$) that was not limited by soil water supply. We adopted this approach solely to determine the influence of an additional groundwater supply; an explicit model of three-dimensional groundwater flow was beyond the scope of the present study. The $S_{SUBSIDY}$ was calculated as $\sum_s E_{pot} - \sum_s E_{rain}$, and it equals the amount of additional transpiration made possible by eliminating water limitation. The expectation was that this subsidy should also maximize stand productivity, which was assessed by the corresponding cumulative canopy photosynthesis ($\sum_s A_{rain}$, $\sum_s A_{pot}$). In stands where $\sum_s E_{rain}$ was insufficient to keep the stand alive (above the 85 PLC mortality threshold by the end of the growing season), we established the minimum transpiration and photosynthesis required for survival ($\sum_s E_{mort}$, $\sum_s A_{mort}$). Finally, we estimated the actual seasonal transpiration and canopy photosynthesis during the modeled (year 2016) growing season ($\sum_s E_{pred}$, $\sum_s A_{pred}$). From these benchmarks we were able to estimate the dependence of nonstressed aspen stands on a root zone subsidy, the critical reduction in subsidy predicted to induce mortality, and the current stress level for the stand.

To evaluate model predictions, we measured tree ring chronologies for each stand and compared them with long-term weather records. We expected that stands requiring large amount of subsidy from groundwater to maximize productivity would grow wider rings following a year of abundant snowpack. Ring widths in non-subsidized stands should be less sensitive to snowpack. We also expected that subsidized stands could be more sensitive to growing season moisture deficit, because they would tend to be stressed during periods of low subsidy. Nonsubsidized stands would be less likely to suffer water stress and hence should show less sensitivity to growing season aridity.

We also compared the model results with the xylem vulnerability curves collected across the 10 stands. These curves measure the loss of hydraulic conductance from xylem cavitation, and they are critical model parameters for calculating hydraulic risk. There can be a strong relationship across species between cavitation resistance and local (Kolb & Sperry, 1999; Lopez et al., 2005; Pockman & Sperry, 2000; Vinya et al., 2013) and larger-scale aridity gradients (Choat et al., 2012; Maherali et al., 2004). In particular, we evaluated whether stands that were more dependent on a subsidy and hence also more likely to be stressed during shortfalls, had xylem that was also more resistant to cavitation. Such patterns of within-species variability in cavitation resistance (e.g., Jacobsen et al., 2014; López et al., 2013; López et al., 2016) may be useful for future model parameterization at landscape and regional scales.

2. Materials and Methods

2.1. Model Overview, Assumptions, and Inputs

The gain-risk model as implemented by Venturas et al. (2018) was run at hourly time steps throughout the 2016 growing season and produced an hourly time course of root-zone water content, plant canopy xylem pressure, plant hydraulic conductance, whole stand transpiration and assimilation rates, and other gas exchange parameters. Boundary conditions were root zone water content at the beginning of the growing season (assumed half the saturated water content for the soil type; Campbell, 1985), and hourly measurements of wind speed, solar radiation, precipitation, air temperature, and atmospheric vapor pressure deficit (D). These hourly data for the 2016 growing season were obtained from stations nearest to the stand and at similar elevation (mesowest.utah.edu, see Horel et al., 2002). Model parameters were measured for 10 aspen stands across the state (Figure 2) from data collected during 10 visits (one per stand) in late July to early September 2016 (Tables 1 and 2; for details on parameter measurements see Text S1 in the supporting information). No stand was riparian, in the sense of being in a valley floor adjacent to a perennial stream, though one (Amasa Valley, AV) was near a spring.
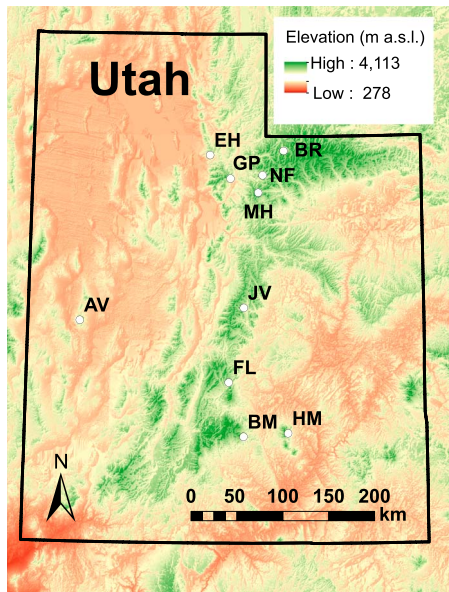
Figure 2. Location and approximate elevation of survey stand locations in Utah, USA. Stand abbreviations, elevation, and other characteristics are given in Tables 1 and 2.

The model requires "vulnerability curves" (VC) for rhizosphere, root, stem, and leaf elements of the continuum. These describe how hydraulic conductance of the element (K) falls from its maximum (K_{max}) as reduced by rhizosphere drying or xylem cavitation as the water pressure (P) becomes more negative:

$$K = K_{max} \cdot f(P) \tag{2}$$

The hydraulic conductance represents the average for trees in these relatively homogeneous stands. The rhizosphere K_{max} was set to achieve an average of 50% resistance in the rhizosphere element, averaged from soil water potential (P_s) of zero to the P_s at hydraulic failure. This setting was based on controlled drought experiments in aspen (Venturas et al., 2018). The rhizosphere vulnerability curve was characterized using the van Genuchten function (van van Genuchten, 1980) for the stand's soil type as assessed from soil texture and corresponding moisture release parameters (α and n). The van Genuchten functions were also used to relate soil water content and P_s, and to determine the volumetric water content of soils at field capacity. The soil was assumed to be free of rocks. Root and stem xylem curves were measured from samples collected on site using the standard centrifuge method (Alder et al., 1997; Tobin et al., 2013; Text S1.2) and represented by a two-parameter Weibull function ($f(P) = e^{-[(P/b)^c]}$, with curve parameters b and c). The leaf vulnerability curve was assumed equal to the stem. Based on model tests with aspen saplings (Venturas et al., 2018), the model was run without xylem refilling, meaning that the reduction in xylem K was permanent. The rhizosphere K was assumed to recover without hysteresis when soil rehydrated.

The xylem element K_{max} was estimated from leaf hydraulic conductance (LSC, per leaf area) measured onsite using the evaporative flux method for intact leafy shoots (Text S1.3). The LSC was scaled to the stand using the leaf area per basal area (LA:BA) as estimated from site branch samples and an average allometric relationship determined for broadleaf tree species (LA proportional to $BA^{0.87}$, Text S1.3; Martin et al., 1998). Whole tree K was estimated by assuming leaves accounted for 25% of whole plant flow resistance (Sack & Tyree, 2005; von von Allmen et al., 2015). Measured tree and leaf K values were used to back-calculate their corresponding K_{max} values based on predawn and midday xylem pressures on the day of LSC measurement. Stem and root K_{max} assumed a 2:1 ratio of tree K_{max} after leaf K_{max} was factored out (Venturas et al., 2018).

The vulnerability curves are used by the model to compute the risk function at each time step. The risk function is calculated by incrementing the instantaneous transpiration rate (E) from E = 0 and solving for canopy P (including the gravitational pressure drop for stand height) until E = E_{crit} is reached, at which point the drop in canopy P has driven the canopy hydraulic conductance to zero. The risk is the fractional loss of canopy hydraulic conductance, which starts from zero when E = 0 and rises to 1 at E = E_{crit}. At the same time, the model calculates the gain function. Each E increment is used to calculate, in order, (1) leaf temperature, (2) leaf-to-air vapor pressure deficit, (3) diffusive conductance to water vapor and CO_2, and (4) instantaneous net assimilation (A) from a Farquhar-type model (Sperry et al., 2017). The A is normalized in a gain function to rise from zero when E = 0 (negative A is set to zero) to 1 when A reaches a maximum (usually at E_{crit}). The point at which the gain-risk difference is maximized provides the canopy P and associated outputs for that time step. The model assumes no effect of prior drought on canopy P but reduces fluxes at that P as calculated from any previous permanent loss of xylem conductance. The gain-risk calculation is then repeated for each subsequent time step. If photosynthetic photon flux density falls below 30 μmol s^{-1} m^{-2}, the stomata are assumed to stay shut; thus, the model assumes no nocturnal transpiration.

The maximum carboxylation capacity (V_{max25}; denoting the 25 °C value) needed to solve for A was estimated as the value providing the best fit to average midday P on the measurement day. The maximum electron transport capacity, J_{max25}, was estimated as 1.67 × V_{max25} (Medlyn et al., 2002), and both V_{max25} and J_{max25} were assumed constant over the growing season. Separate gain functions were computed for sun and shade canopy layers based on the light penetration model outlined by Campbell and Norman (1998));

Table 1
Stand Physical Characteristics and Climatic Data for 1901–2016 Mean and for 2016

Stand ID	Stand name	Coordinates (Datum WGS84)	Elevation (m)	Soil type (α, n)	Mean AP (mm)	Mean AT (C°)	2016 AP (mm)	Mean PAS (mm)	2016 PAS (mm)	Mean CMD (mm)	2016 CMD (mm)	Mean GSP (mm)	2016 GSP (mm)	2016 Midday VPD (kPa)
AV	Amasa Valley	39.172333 N 113.392611 W	2,622	Loam (367.35, 1.56)	440	7.8	510	105	118	502	550	101	74	3.1
BM	Boulder Mountain	38.047028 N 111.324472 W	2,878	Organic matter[a] (367.35, 1.56)	519	4.1	508	196	197	386	466	205	150	3.0
BR	Bear River	40.853583 N 110.821167 W	2,676	Loam (367.35, 1.56)	696	1.7	718	408	415	378	442	211	165	4.0
EH	Elk Hollow	40.811917 N 111.768194 W	2,032	Loam (367.35, 1.56)	749	6.7	787	218	201	450	487	209	181	2.9
FL	Fish Lake	38.580306 N 111.512500 W	2,780	Clay Loam (193.87, 1.31)	518	3.8	520	212	233	401	477	192	139	1.5
GP	Guardsman Pass	40.581861 N 111.502861 W	2,457	Loam (367.35, 1.56)	741	4.7	776	336	334	393	451	187	145	4.4
HM	Henry Mountains	38.082056 N 110.769944 W	2,826	Clay Loam (193.87, 1.31)	612	4.2	626	252	257	376	452	210	159	2.1
JV	Joes Valley	39.313250 N 111.326167 W	2,612	Silty Clay Loam (102.04, 1.23)	593	3.7	627	270	322	395	464	191	142	1.6
MH	Mill Hollow	40.443222 N 111.146306 W	2,718	Clay Loam (193.87, 1.31)	832	2.0	877	500	533	349	415	222	170	2.7
NF	Norway Flat	40.614639 N 111.091000 W	2,564	Loam (367.35, 1.56)	742	3.2	776	397	407	416	483	199	152	3.4

Note. AP = annual precipitation; AT = annual temperature; PAS = annual water year (August–July) precipitation as snow; CMD = climatic moisture deficit during the growing season (May–September); GSP = growing season precipitation (May–September); VPD = midday (11:00–13:00) vapor pressure deficit during the growing season.
[a]For stand BM, only organic matter was obtained in the soil sample and the parameters for loam soil were used in model simulations

Table 2
Stand Plant Traits

Stand ID	BA:GA (m²/ha)	LA:BA (m²/m²)	Height (m)	Age (years)	PD (−MPa)	MD (−MPa)	LSC (mmol s⁻¹ m⁻² MPa⁻¹)	Stem VC (b, c)	Root VC (b, c)	V_{max25} (μmol m⁻² s⁻¹)	Tree K_{max} (kg h⁻¹ MPa⁻¹ m⁻²)	Stand LAI (m²/m²)
AV	142.7	760 ± 69[b]	16.3 ± 0.8[bcd]	98 ± 7[abc]	0.40 ± 0.05	1.49 ± 0.13	3.5 ± 0.8[bcd]	1.79, 0.94	1.03, 1.01	47.0	73.6	2.38
BM	14.9	1410 ± 70[a]	9.0 ± 0.3[e]	37 ± 2[e]	0.36 ± 0.02	1.90 ± 0.04	3.7 ± 0.7[bcd]	2.53, 1.32	1.03, 0.84	55.1	137.5	1.43
BR	80.7	980 ± 88[b]	16.4 ± 0.8[BC]	115 ± 1[a]	0.55 ± 0.05	1.73 ± 0.21	8.4 ± 1.4[a]	2.55, 1.27	1.46, 1.36	66.1	203.1	1.54
EH	26.9	819 ± 48[b]	18.3 ± 1.4[ab]	60 ± 1[de]	0.34 ± 0.02	1.84 ± 0.29	1.2 ± 0.4[d]	4.08, 1.56	0.78, 0.72	34.6	26.2	1.39
FL	26.0	982 ± 41[b]	8.4 ± 0.2[e]	106 ± 12[abc]	0.64 ± 0.05	1.65 ± 0.04	7.0 ± 0.4[ab]	3.73, 2.00	1.37, 1.42	99.6	191.5	0.71
GP	12.3	897 ± 128[b]	11.7 ± 1.6[de]	45 ± 4[e]	0.27 ± 0.02	1.55 ± 0.05	2.3 ± 0.4[cd]	2.71, 3.24	0.90, 0.76	85.4	47.9	0.56
HM	77.3	983 ± 72[b]	12.8 ± 1[e]	123 ± 12[a]	1.09 ± 0.05	1.86 ± 0.05	6.3 ± 1.2[ab]	4.72, 2.13	1.71, 1.31	62.4	224.7	1.45
JV	43.9	874 ± 81[b]	11.6 ± 0.5[e]	83 ± 7[bcd]	0.86 ± 0.11	1.51 ± 0.05	3.3 ± 0.5[bcd]	2.99, 2.21	2.33, 1.14	23.0	78.2	1.32
MH	44.9	1105 ± 104[ab]	19.0 ± 1.1[ab]	80 ± 4[cd]	0.33 ± 0.02	1.74 ± 0.10	1.2 ± 0.4[d]	2.98, 1.55	0.84, 0.90	32.2	31.7	0.90
NF	45.7	968 ± 62[b]	22.9 ± 1.1[a]	110 ± 2[ab]	0.36 ± 0.01	1.43 ± 0.05	5.6 ± 0.8[abc]	3.74, 1.60	1.14, 1.20	50.9	111.2	0.72

Note. When appropriate the standard error of the mean (±SE) is reported as well as significance letters based on a Tukey HSD test. BA:GA = basal area to ground area ratio; LA:BA = leaf area to basal area ratio; PD = predawn xylem pressure; MD = midday xylem pressure; LSC = leaf specific conductance; Stem VC = stem xylem vulnerability curve b and c parameters; Root VC = root xylem vulnerability curve b and c parameters; V_{max25} = maximum carboxylation rate at 25°C; Tree K_{max} = maximum whole tree conductance per basal area; Stand LAI = stand leaf area index obtained from hemispheric photographs.

see also Venturas et al. (2018). The light model required a stand leaf area index (LAI) which was calculated from hemispheric photographs using Gap Light Analyzer software (Frazer et al., 1999). LAI was also assumed constant over the growing season.

Between hourly time steps, the root-zone water content and P_s were updated based on the net flux from each of five soil layers. Layer depths were set for equal root biomass (assumed proportional to absorbing root area) according to

$$M = 1 - B^d \tag{3}$$

where M is the fraction of root biomass above depth d (in cm), and B is a coefficient (0–1) set from the maximum rooting depth (d at M = 0.995). Average root depth was set to 1.25 m, with a range from 0.5 to 2 m (Gifford, 1966). Net flux per layer was the sum of (1) root withdrawal, (2) root efflux in the case of root-mediated redistribution (flux into the layer is negative), (3) rain infiltration, and (4) vertical losses or gains to adjacent horizontal layers via soil transport.

Root fluxes (1 and 2) were scaled to a ground area basis based on the basal area per ground area of the stand (BA:GA; Text S1.1). Understory vegetation was not modeled because it was scarce and represented a small proportion of total living biomass. Rain (flux 3) was assumed to infiltrate soil to field capacity from the surface down, with no loss to interception, runoff, or lateral subsurface flow. Vertical fluxes between soil layers (flux 4) included losses to soil surface evaporation and a subsidy simulated as vertical flow into the root zone from a water table. Soil evaporation was modeled from a 2-cm-thick surface layer devoid of roots (see Venturas et al., 2018). To control the subsurface subsidy, an optional water table ($P_s = 0$) was set to a specified depth below the root zone. Soil flow between layers was estimated as the integral over ΔP_s between layers of the van Genuchten soil conductivity function, with K_{max} corresponding to the vertical distance between layer midpoints (or to the water table surface in the case of rise into the root zone).

The beginning of the growing season was determined from thermal time (Fu et al., 2012) calculated as the cumulative degree-days above 5 °C from 1 February 2016. Budburst was assumed to coincide with the abrupt increase seen in cumulative degree-days during spring (occurring at 165 degree-days on average, range 110–250). Simulations ended on the last day of September 2016.

2.2. Simulating Root Supply Versus Canopy Function

For each stand, cumulative seasonal stand transpiration ($\sum_s E$, mm per season), was predicted as a function of root-zone water input. An input of zero meant the stand could only use the water locally stored in the root zone at the start of the season (source S_{SOIL} in equation (1)). The initial nonzero input corresponded to 2016 growing season precipitation without any subsurface subsidy ($S_{SOIL} + S_{PPT}$ sources). This rain-only simulation yielded the corresponding cumulative stand transpiration ($\sum_s E = \sum_s E_{rain}$, mm per season). Inputs above growing season rainfall were achieved by adding a water table perched beneath the root zone ($S_{SOIL} + S_{PPT} + S_{SUBSIDY}$ sources). Water table depth was constant over a growing season simulation, but was progressively raised between simulations until stand $\sum_s E$ reached its maximum potential rate ($\sum_s E_{pot}$, mm per season). The $S_{SUBSIDY}$ term was quantified by the increase in seasonal transpiration achieved by eliminating the water

limitation ($\sum_s E_{pot} - \sum_s E_{rain}$) as a percentage of maximum potential transpiration (% $S_{SUBSIDY}$):

$$\%S_{SUBSIDY} = 100 \cdot \frac{\left(\sum_s E_{pot} - \sum_s E_{rain}\right)}{\sum_s E_{pot}} \qquad (4)$$

Root zone inputs low enough to induce stand mortality (at $\sum_s E = \sum_s E_{mort}$, millimeters per season) were based on the 85 PLC mortality threshold identified for aspen by Venturas et al. (2018). The actual transpiration of each stand in 2016 ($\sum_s E_{pred}$) was estimated by matching measured predawn xylem pressure with simulated predawn xylem pressure for the same day.

To assess the relationship between stand water use benchmarks ($\sum_s E_{pot}$, $\sum_s E_{pred}$, $\sum_s E_{mort}$, and $\sum_s E_{rain}$) and productivity we also determined the associated values for seasonal canopy net photosynthesis ($\sum_s A$, kg C season^{-1} m^{-2} ground area), a proxy for stand productivity. The corresponding values for soil-to-canopy hydraulic conductance and the end of the growing season (K_{tree}, kg h^{-1} MPa^{-1} m^{-2} basal area) indicated the role of vascular transport capacity in limiting canopy fluxes.

To assess uncertainty in model output, we bootstrapped major model inputs 100 times for $\sum_s E_{pot}$, $\sum_s E_{rain}$, and % $S_{SUBSIDY}$ outputs (sample size was limited by computing time required). The 95% confidence intervals around the bootstrapped mean outputs were estimated from percentiles (2.25th and 97.25th). Where possible, inputs were bootstrapped with replacement from the measured sample size (LA:BA, LSC, xylem VCs, tree height, the same inputs were bootstrapped at every stand). The BA:GA was a single measurement and was bootstrapped over a ±10% range. Maximum root depth was bootstrapped from 0.5 to 2 m. Although we did not bootstrap the initial soil water content per volume (field capacity), bootstrapping the root depth varies the total water content accessible by roots. The bootstrapped range for estimates of V_{max25}, % rhizosphere resistance, and % resistance in the leaf was ±20%. Bootstrapping included K_{max} values through their dependence on bootstrapped LA:BA, LSC, and % resistance in the leaf.

2.3. Tree Ring Analysis

Tree cores collected from a minimum of 10 overstory ramets at each site were processed, cross-dated, and measured for ring width using standard methods at the Utah State Dendrochronology Laboratory (Text S1.4; Bunn, 2010; Holmes, 1983; Stokes & Smiley, 1996). For each chronology we analyzed the correlation of annual ring width index with annual precipitation as snow (PAS) and Hargreaves climatic moisture deficit (CMD, mm, summed from May through September) for chronologies of 20 to 114 years prior to 2016. The CMD integrates the effect of annual precipitation and vapor pressure deficit. The PAS and CMD records were estimated from 4 km gridded climate data (years 1901–2016) generated using the ClimateNA v5.10 software package (http://tinyurl.com/ClimateNA, based on methodology described by Wang et al., 2016). We quantified the Pearson correlation coefficient for 1,000 bootstrapped replicates of ring width to estimate stand sensitivity to climate using the R package "treeclim" (Zang & Biondi, 2015).

2.4. Relationships Between Cavitation Resistance, Climate, and Modeled Water Status

Cavitation resistance was quantified by the pressure at 50% loss in conductivity (P50) based on the Weibull function vulnerability curves of stems and roots at each site. Significant differences between P50's were determined by ANOVA. Where significant differences were identified, we determined significant inter-stand differences using a Tukey HSD test. Correlation between P50 and climate were assessed using Pearson correlation in the R software package (R Core Team, 2016). Six site-specific climatic variables were tested: (1) mean 2016 midday (11:00–13:00 MST) vapor pressure deficit (VPD) during the growing season, (2) cumulative 2016 rainfall during the growing season (GSP, mm), (3) precipitation as snow (PAS, mm) averaged from 1901–2016, (4) average annual (1901–2016) Hargreaves climatic moisture deficit (CMD, mm, summed from May through September), and (5) average annual (1901–2016) precipitation (mean AP, mm, summed from January through September), (6) average annual (1901–2016) temperature (mean AT, °C, from January through September). In addition, we tested for significant relationships between P50 and measured stand predawn xylem pressure, and whether stands were predicted to be "stressed" (i.e, with $\sum_s E_{pred}$ greater than $\sum_s E_{mort}$, but less than $\sum_s E_{pot}$) versus "nonstressed" ($\sum_s E_{pred} = \sum_s E_{pot}$) using logistic regression.
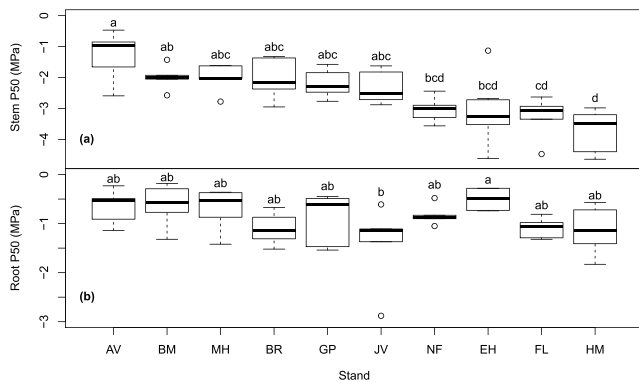
Figure 3. Box and whisker plots of variability in stem and root xylem pressure at 50% loss of hydraulic conductivity (P50) across aspen stands (abbreviations in Table 1). Letters denote significant differences between stands based on a Tukey HSD test. Whiskers represent the upper and lower values within 1.5*IQR (interquartile range) for each stand ($n = 6$). Outliers depicted as open symbols. (a) Stem P50 varied between stands with stands distinctly more vulnerable (AV) and more resistant (HM). (b) Root P50 showed only a single significant difference between stands JV and EH.

3. Results

3.1. Model Parameters

The modeled 2016 growing season was drier than normal in terms of precipitation (74–181 mm) and CMD (415–550 mm; Table 1; hourly model weather inputs in Data Set S1). The climatically driest stand was AV in the more arid western part of Utah. The wetter stands were generally in the northern mountain ranges (Figure 2 and Table 1). Stand structure varied an order of magnitude in basal area per ground area, leaf area per basal area, and stand height (Table 2). Photosynthetic and hydraulic capacities were more consistent but still showed significant variation between stands (Table 2). The V_{max25} averaged 55.4 µmol s^{-1} m^{-2} (Table 2) based on the best fit to midday xylem pressure (mean absolute error of 0.19 MPa).

Aspen stems were significantly more resistant to cavitation than roots in nine out of 10 stands (P ranged from 0.03 to <0.0001, t test), the exception being stand AV ($P = 0.11$). Stands exhibited a range of stem cavitation resistance, with P50 values from -1.21 to -3.98 MPa (averaging -2.57; Figure 3a). There was less variability in root P50 (-0.57 to -1.69 MPa), and only two sites (Elk Hollow, EH, and Joes Valley, JV) were significantly different (Figure 3b).

3.2. Root Supply Versus Canopy Function and Subsidy Estimation

Simulations from stand HM (Henry Mountains) illustrate the process of generating each stand's relationship between root zone water supply and canopy function. A single simulation yielded a growing season time course of daily stand transpiration ($\sum_d E$, mm day^{-1}; Figure 4) for a given root zone input scenario with 2016 atmospheric conditions. Summing $\sum_d E$ and total root zone input over the season (mm per season), yielded one point on the plot of seasonal E ($\sum_s E$) versus water supply (Figure 5a). The same process gave seasonal net assimilation ($\sum_s A$), and end-of-season K_{tree} (Figures 5b and 5c). The most important simulations for estimating the root zone subsidy were (1) root zone initialized at field capacity and 2016 growing season precipitation with no subsidy (Figure 4, blue-red line simulation, and Figures 5a–5c, $\sum_s E_{rain}$, $\sum_s A_{rain}$, and K_{rain}) and (2) sufficient additional subsidy to maximize stand E (Figure 4, black line, and Figures 5a–5c, $\sum_s E_{pot}$, $\sum_s A_{pot}$, K_{pot}).

In the case shown, summer rain and stored water were not sufficient to keep the HM stand alive because $\sum_d E$ fell sharply (by day 170) and the stand crossed the 85% loss in hydraulic conductance (PLC) mortality threshold by day 177 (Figure 4, blue-to-red line transition; Figure 5c, K_{mort} threshold). Rain events (cyan bars) had a limited effect despite increasing soil P_s (e.g., after day 183), because of the legacy of reduced plant hydraulic conductance caused by xylem cavitation. When a large enough subsidy was fed into the rooting zone, $\sum_d E$ became maximized (Figure 4, black line), which was summed to give the $\sum_s E_{pot}$ (Figure 5a). Daily variation in this maximum $\sum_d E$ was mainly driven by light intensity and atmospheric vapor pressure deficit (D). This can be seen in notable drops in transpiration during large rain events (e.g., Figure 4, day 183) when light and D were much lower than on sunny days when $\sum_d E$ is limited by stand hydraulic conductance. Additional simulations filled in the gap between $\sum_s E_{rain}$ and $\sum_s E_{pot}$, allowing the thresholds for mortality to be estimated (Figures 5a–5c, $\sum_s E_{mort}$).

The trajectory of $\sum_s A$ and K with root water supply followed a similar trajectory as $\sum_s E$ with all becoming saturated at a similar "water-limiting threshold" (Figures 5a–5c, $\sum_s E_{pot}$, $\sum_s A_{pot}$, and K_{pot}). This result indicates that peak water use corresponds with peak canopy photosynthesis (and by
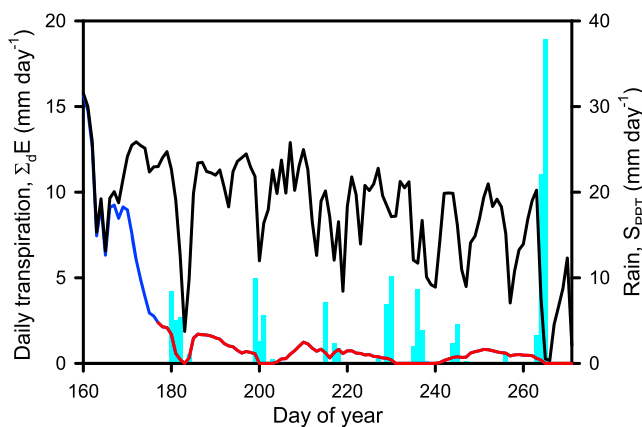

Figure 4. Daily transpiration as modeled for Henry Mountains stand (HM) 2016 growing season. The blue trace depicts daily transpiration ($\sum_d E$, mm/day) under a rain input only scenario (plus initial root zone water content, $S_{SOIL} + S_{PPT}$ from equation (1)). Rainfall (cyan bars) is insufficient to prevent the stand from crossing the mortality threshold (red line) based on an 85% reduction in soil-canopy hydraulic conductance. The black trace depicts the stand with a subsidy sufficient to maximize cumulative seasonal transpiration. Fluctuations are correlated with decreases in light and vapor pressure deficit during rain events.
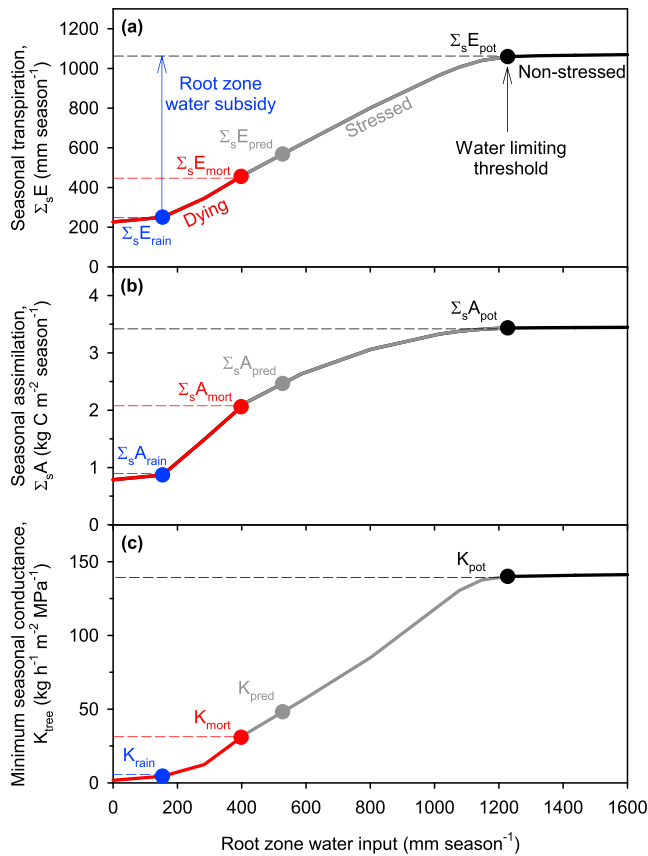
Figure 5. Root supply versus canopy function for the Henry Mountains stand (HM). Root zone water supply is cumulative amount per season. (a) Cumulative seasonal transpiration ($\sum_s E$). Input above the water-limiting threshold (black arrow and circle) is sufficient to maximize transpiration and eliminate stand water stress ($\sum_s E_{pot}$, "nonstressed"). Reduced input decreases $\sum_s E$ and results in "stressed" stands. When stress causes the soil-canopy hydraulic conductance to fall by 85% or more, the stand is at high risk of mortality ($\sum_s E_{mort}$, red symbol, "dying"). The transpiration rate sustained by stored water and growing season precipitation ($\sum_s E_{rain}$) is shown with a blue symbol. The difference between $\sum_s E_{pot}$ and $\sum_s E_{rain}$ (blue subsidy arrow) indicates the need for an additional water subsidy to eliminate stand water stress. The predicted stand location ($\sum_s E_{pred}$) based on survey predawn pressure measurement is noted with a gray-filled circle. (b) Cumulative net assimilation ($\sum_s A$) per ground area. The $\sum_s A_{pot}$, $\sum_s A_{mort}$, $\sum_s A_{rain}$, and $\sum_s A_{pred}$ for the corresponding $\sum_s E$ benchmarks are shown. (c) End of season minimum soil-canopy hydraulic conductance (K_{tree}). The K_{pot}, K_{mort}, K_{rain}, and K_{pred} for the corresponding $\sum_s E$ benchmarks are indicated.

proxy the productivity) and that both are associated with avoiding loss of soil-to-canopy hydraulic conductance from water stress. The water-limiting threshold (Figure 5a, arrow) is the minimum root zone water supply required to prevent a significant loss of stand water conducting capacity over the growing season.

The magnitude of seasonal $\sum_s E$ indicated the health and photosynthesis of the stand with respect to water status. "Nonstressed" stands were at $\sum_s E_{pot}$ with minimal water stress and maximum assimilation. "Stressed" stands are between $\sum_s E_{pot}$ and $\sum_s E_{mort}$, experiencing significant, but nonlethal water stress and reduced assimilation. "Mortality" stands are below $\sum_s E_{mort}$ and are expected to suffer death by drought. In the case shown, stand HM was estimated to fall within the stressed zone (Figure 5, gray circle) based on its measured predawn xylem pressure (Table 2). The relationship of $\sum_s E_{pot}$ to $\sum_s E_{rain}$ enabled the estimation of the subsidy under optimal conditions (% $S_{SUBSIDY}$; equation (4); Figure 5, upward blue arrow, analogous calculations can be performed for $\sum_s A$).

Six of the 10 stands had a $\sum_s E_{pot}$ well above $\sum_s E_{rain}$ (Figure 6a), and hence required a significant subsidy (Figure 6c). The average % $S_{SUBSIDY}$ was 54% (range: 31% to 78%; Figure 6c). The corresponding percentage of maximum assimilation averaged 52% (range: 32% to 76%; Figure 6b). Five of these six stands were not projected to survive on rain alone (Figure 6a, $\sum_s E_{mort} > \sum_s E_{rain}$). Four of these six stands were estimated as "stressed" during the 2016 growing season (Figures 6a and 6b, circles); the remaining two stands were "nonstressed" (symbols not shown). Four of the 10 stands had $\sum_s E_{pot} = \sum_s E_{rain}$ (Figure 6a), meaning they had a low enough demand for water ($\sum_s E_{pot} \leq 141$ mm per season) that they were never limited even if only supplied with stored water and growing season precipitation. These stands were all estimated to be "nonstressed" and at their $\sum_s E_{pot}$.

The major determinant of $\sum_s E_{pot}$, and hence the dependence on a subsidy, was stand level K_{max} (K_{max} per ground area = K_{max} per basal area multiplied by BA:GA; Figure 7). Stand K_{max} explained 94% of the variation in $\sum_s E_{pot}$ (Figure 7). Dense stands of high conductance trees had greater maximum demand for water, and hence required a greater subsidy.

3.3. Tree Ring Analysis

Over time the six subsidized stands showed a strong tendency for ring width to be positively correlated with precipitation as snow (larger growth rings with increasing PAS; Figure 8a) and negatively correlated with climatic moisture deficit (narrower rings with increasing CMD; Figure 8b). Nonsubsidized stands were relatively insensitive to either metric. The pattern emerged more recently for PAS, becoming evident in five of the six subsidized stands within 35 years and in all six subsidized stands by 100 years. At a given time, there was at most only one nonsubsidized stand sensitive to PAS. The CMD relationship was less widespread and emerged more slowly with five of six subsidized stands becoming sensitive by 100 years. From 35 years on, none of the nonsubsidized stands were sensitive to CMD. Only EH stand showed a significant correlation with CMD for 20- to 30-year-long chronologies, but they were opposite to expected as it was a positive correlation (i.e., they showed wider growth rings on years with larger CMD).

3.4. Relationships Between Cavitation Resistance, Climate, and Modeled Water Status

Cavitation resistance tended to increase with modeled and measured indicators of stand water stress. There was a significant association between "nonstressed" versus "stressed" stands (as distinguished in Figure 6)
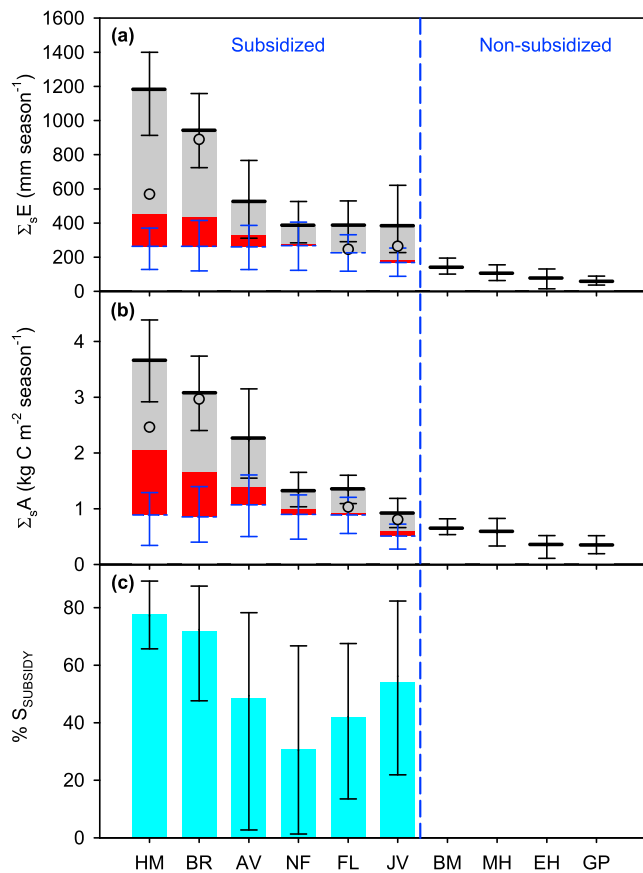
Figure 6. (a) Stand estimates for season transpiration ($\sum_s E$). Upper limit (heavy black line) is the maximum achieved by subsidizing the root zone ($\sum_s E_{pot}$) and the lower limit (blue dashed line) is the value for rain and stored water alone ($\sum_s E_{rain}$). Corresponding error bars are bootstrapped 95% confidence intervals (CI). Transition between stressed (gray) and dying (red) stands is the mortality threshold ($\sum_s E_{mort}$). Stands with $\sum_s E_{pot} > \sum_s E_{rain}$ were "subsidized" and the four stands with $\sum_s E_{pot} = \sum_s E_{rain}$ were "nonsubsidized". Four of the 10 stands were estimated to be in the stressed zone between $\sum_s E_{pot}$ and $\sum_s E_{mort}$ (circles); the remaining stands were estimated to be at $\sum_s E_{pot}$. (b) Same graph as in (a), but for season net assimilation per ground area ($\sum_s A$). (c) The % $S_{SUBSIDY}$ for each stand was computed from equation (4) with 95% CI.

and increasingly negative P50 (root and root + stem average P50 $P < 0.001$, stem P50 $P < 0.05$; logistic regressions). Likewise, stands with more negative predawn xylem pressure had significantly more negative root P50 and average root + stem P50 ($r^2 = 0.75$ and 0.60, respectively; $P < 0.01$; not significant for stem P50). Cavitation resistance was not correlated with any climate drivers (Mean AP, Mean AT, PAS, and CMD) as calculated from the mean stand climate over years 1901–2016, or for 2016 growing season precipitation or VPD. Climate drivers were also not related in any detectable way to stand water status ("nonstressed" vs. "stressed") or predawn xylem pressure.

4. Discussion

The model predicted that a majority of the aspen stands required a significant amount of subsidy to the root-zone to minimize water stress and maximize assimilation. When only relying on root zone storage and incident summer rain, half of the stands would be at risk of mortality (Figure 6). This dependence on groundwater subsidy was also supported by the tree ring chronology, which showed a significant correlation with winter precipitation as snow in subsidized stands (Figure 8). These findings are consistent with previous studies in snow-dominated environment suggesting soil recharge during wintertime provides an important water source for sustaining plant water use during the growing season (Bigler et al., 2007; Fritts, 1974; Hanson & Weltzin, 2000; Williams et al., 2013). Although the modeling results pertain specifically to the 2016 season, summer rain is quite limited in these forests (based on PRISM climate record from 1901 to 2016; Table 1) and would be unlikely to ever provide the amount of water required to achieve the large $\sum_s E_{pot}$ (>141 mm per season; Figure 6a) in subsidized stands. Because of the link between winter snowpack and groundwater recharge in the montane ecosystems where aspen forests occur in Utah (Castle et al., 2014; Garreaud et al., 2017; Maurer & Bowling, 2014), a major implication of the results is that subsidized aspen forests in the intermountain region of the United States could be much more vulnerable to reductions in winter precipitation than to summer drought.

Most of the simplifying assumptions required to model the complexities of stand water balance would result in a conservative estimate of the subsidy. The generous root-zone depth range (0.5 to 2 m), and assumed absence of rocks, would tend to 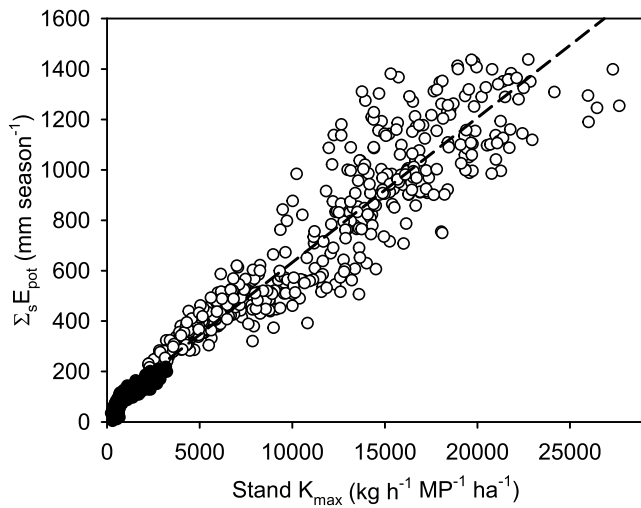maximize the availability of local soil moisture per tree. We started simulations assuming initial stored water was at field capacity rather than saturation, which is reasonable considering relative water content measurements in other Utah montane stands (Maurer & Bowling, 2014). A sparse snowpack and early melt could even prevent field capacity from being reached prior to bud break. Rain infiltration was maximized by assuming no interception or runoff. Soil evaporation represented a mean loss of 51.3% of growing season precipitation (GSP) across stands, ranging from 19.0% for AV to 69.5% for EH. This relatively high proportion of GSP lost to soil evaporation is due to rain events being infrequent and of small magnitude, which resulted in the rain not penetrating the soil beyond the 2-cm layer of surface soil. The absence of any understory allowed aspen sole access to root zone water content. Generous error in input estimates (e.g., ±20%) propagated to broad confidence intervals on model output (Figure 6). Regardless of these settings, the predicted reliance on ground subsidy was significant. Summer rainfall was simply too sparse in these stands to sustain transpirational demands much above 141 mm per season without additional water supply.

Previous research on aspen mortality in Colorado, USA, supports the importance of soil water redistribution and indicates that the magnitude of the subsidy may be influenced by local topography. Tai et al. (2017)

Figure 7. Maximum seasonal stand transpiration ($\sum_s E_{pot}$) versus maximum stand hydraulic conductance (stand K_{max} per ground area) obtained by bootstrapping (100 values per stand). The black dashed line is a significant linear regression ($R^2 = 0.94$, $P < 0.001$). Open circles represent subsidized stands, and black closed circles nonsubsidized stands.

found that aspen stands located in topographically divergent areas (i.e., ridges) generally exhibited higher mortality compared to neighboring water-collecting convergent areas (i.e., valleys), in response to a severe multiyear drought (2000–2003). The anomalously hot and dry summers during this drought appear to have exacerbated aspen mortality in southwestern Colorado (Anderegg et al., 2013). This region is well inside the track of the southwestern monsoon and summer rain is normally more abundant than in the modeled Utah stands (Adams & Comrie, 1997), possibly leading to growth of more rain-dependent stands. Any shortfall in the subsurface subsidy would also amplify the effects of a dry summer on normally subsidized stands. Indeed, four of the subsidized Utah stands were estimated to be stressed in 2016, whereas all of the nonsubsidized ones were nonstressed. Tree ring chronologies of subsidized stands also tended to be more sensitive to the climatic moisture deficit during the growing season than nonsubsidized ones (Figure 8b).

Although our evidence for aspen stands relying on groundwater subsidy is strong, the mechanism of its delivery is not explicitly resolved. Although we modeled the subsidy as upward flux from a static water table, this was a convenient substitute for what is likely to be a much more complex situation. In actuality, the subsidy could be arriving via any combination of vertical and lateral flow, within and below the root zone, and from a variety of precipitation events over a range of periods. It could also be delivered from a few deep roots tapping bedrock-bound aquifers. While most aspen roots are concentrated in the upper 1.5 m of soil, aspens have been observed to have "sinker roots" that can tap deeper water sources (Gifford, 1966). This trait may be supporting populations of aspen stands in regions that are more prone to persistent drought or with

(a)

		Annual Precipitation as Snow (August - July)									
		Maximum chronology length (years)									
		20	25	30	35	40	45	50	75	100	114
Non-subsidized	BM	0.54	0.56	0.56	0.47	0.13	0.13	0.10	0.10	0.09	0.14
	EH	0.12	0.13	0.12	0.24	0.25	0.30	0.29	0.14	0.14	0.14
	GP	-0.20	-0.18	-0.08	-0.02	0.06	0.05	0.05	-0.03	-0.03	-0.03
	MH	0.30	0.23	0.22	0.27	0.25	0.21	0.24	0.24	0.26	0.29
Subsidized	AV	0.48	0.46	0.32	0.38	0.31	0.40	0.40	0.39	0.35	0.32
	BR	0.20	0.13	0.00	0.09	0.08	0.01	0.05	0.10	0.20	0.23
	FL	0.52	0.51	0.47	0.54	0.55	0.56	0.56	0.47	0.42	0.40
	HM	0.64	0.65	0.53	0.56	0.55	0.54	0.50	0.44	0.43	0.42
	JV	0.34	0.33	0.33	0.40	0.37	0.37	0.35	0.24	0.24	0.23
	NF	0.28	0.31	0.29	0.34	0.25	0.24	0.27	0.24	0.31	0.30

(b)

		Hargreaves Climatic Moisture Deficit (May - September)									
		Maximum chronology length (years)									
		20	25	30	35	40	45	50	75	100	114
Non-subsidized	BM	-0.37	-0.17	-0.12	-0.02	-0.05	-0.07	-0.01	-0.04	-0.09	-0.08
	EH	0.58	0.48	0.41	0.20	0.20	0.25	0.25	0.20	0.20	0.20
	GP	0.20	0.13	0.07	-0.02	0.02	0.05	0.03	0.09	0.09	0.09
	MH	-0.05	-0.10	-0.09	-0.17	-0.17	-0.15	-0.19	-0.09	-0.03	-0.07
Subsidized	AV	0.11	0.09	0.12	0.04	0.01	-0.06	-0.13	-0.16	-0.10	-0.11
	BR	-0.41	-0.48	-0.36	-0.35	-0.33	-0.29	-0.32	-0.20	-0.23	-0.23
	FL	-0.15	-0.11	-0.20	-0.27	-0.22	-0.28	-0.33	-0.20	-0.25	-0.24
	HM	-0.22	-0.20	-0.21	-0.31	-0.28	-0.31	-0.38	-0.29	-0.31	-0.33
	JV	-0.29	-0.16	-0.16	-0.20	-0.19	-0.19	-0.23	-0.12	-0.21	-0.18
	NF	-0.02	-0.16	-0.18	-0.23	-0.21	-0.19	-0.22	-0.19	-0.23	-0.19

Figure 8. Significance of correlation between tree ring width for chronologies of indicated length (prior to 2016) and (a) the annual precipitation as snow (PAS) or (b) growing season Hargreaves climatic moisture deficit (CMD). Pearson correlation coefficients are shown for subsidized versus nonsubsidized stands. Significant correlation coefficients ($P < 0.05$) are highlighted in bold, with green shading indicating a positive correlation (i.e., wider rings for years with higher PAS or CMD) and red shading a negative correlation.
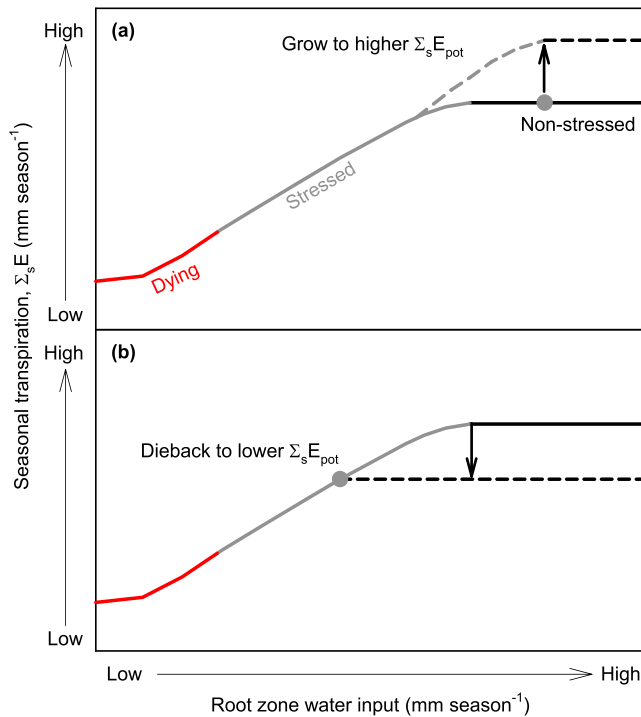
Figure 9. Conceptual diagram of how root supply versus canopy function curves depicted in Figure 5 can predict the optimal response of stands to chronic shifts in root zone water input. Black line means the no stress zone, gray the stress zone, and red the dying zone. (a) A stand with a root zone water input above (gray-filled circle) its water-limiting threshold (black-to-gray transition) has a water surplus. This stand can increase its maximum transpiration rate ($\sum_s E_{pot}$) without causing stress until the root supply becomes limiting (upper dashed line). (b) A stand with a limiting root zone water input (gray-filled circle) is water stressed. This stand can eliminate stress by reducing $\sum_s E_{pot}$ (via controlled dieback) and establishing a lower water-limiting threshold.

shallower and rockier soil that cannot store much water. Given the magnitude of the subsidy (Figure 6), the paucity of summer rain, and the relative abundance of winter precipitation (Table 1), the subsidy is more likely sourced from winter rather than summer precipitation. This expectation is consistent with tree ring widths being positively associated with precipitation as snow in our subsidized stands (Figure 8a). More insight into stand water supply and its origin (winter vs. summer precipitation, aquifer) could be obtained by matching stable isotopes of oxygen and hydrogen between tree and water source (Barbeta & Peñuelas, 2017; Ehleringer & Dawson, 1992; Hu et al., 2010; Snyder & Williams, 2000; West et al., 2012).

The buffering effect of a root zone subsidy on stand water stress is consistent with the decoupling of cavitation resistance from the stand's local climate. Stand AV, for example, is one of the climatically driest locations (Table 1), yet its trees had the most cavitation-prone stem xylem (Figure 3a). However, its vulnerable xylem was consistent with it being a "nonstressed" stand that required, and obtained, a large subsurface subsidy (Figure 6). It was also the only stand with an obvious nearby groundwater source (a small spring). Stand HM, by contrast, had the most cavitation-resistant stem xylem, which was consistent with its being one of the most undersupplied and stressed stands (Figures 5 and 6a). Cavitation resistance and water stress were thus found to be correlated, but neither was in any detectable way associated with stand climate. The more relevant factors determining water stress is the stand structure (i.e., stand K_{max} and $\sum_s E_{pot}$) and the amount of subsidy delivered to the roots.

The relationship of root supply to canopy function depicted in Figure 5 reveals a "water-limiting threshold" of root zone water availability that is just sufficient to alleviate water stress and achieve $\sum_s E_{pot}$ and $\sum_s A_{pot}$ (Figure 5, water limited threshold arrow). While this threshold may not be as well defined in a rain supplied system as in our subsidy-driven situation, it still represents an ecologically and hydrologically significant benchmark. Ecologically, to optimize growth and minimize water stress, stands should develop over time so as to remain somewhat above this threshold (Figure 9) by adjusting stand K_{max} and hence $\sum_s E_{pot}$ (Figure 7). This resembles Eagelson's concept of the long-term equilibrium between plant available water and the abundance of transpiring plants (Cabon et al., 2018; Eagleson, 1982). But the concept also provides a framework for charting long-term forest growth or dieback in response to water availability. Stands operating too far above the threshold over multiple years, with a perennial surplus of water, have the opportunity to add more foliage without increasing their water stress. Hence, they should grow to increase stand K_{max} and $\sum_s E_{pot}$ until the water-limiting threshold is approached (Figure 9a) or another resource besides water becomes limiting (i.e., light or nutrients). Stands operating consistently below their threshold are "victims of their success." They have grown to a high threshold in response to former water availability, but any subsequent shortfall induces physiological stress. These stands should respond by reducing stand K_{max} and $\sum_s E_{pot}$, by partial dieback, to reach a lower threshold and eliminate water stress (Figure 9b). Should the stand fall within the mortality zone, it would have passed the point of no return and be unable to recover.

Hydrologically, the water-limiting threshold corresponds to the transition between transpiration limited by water supply and transpiration limited by the evaporative gradient ("energy limited"). The Budyko curve describes this transition for long-term water balance at the catchment scale: When catchment evapotranspiration (ET) equals its potential evapotranspiration (PET), the system is energy limited, but too little precipitation will make ET fall short of PET (Zhang et al., 2001). Despite the conceptual overlap with Budyko theory, our root supply versus canopy function curves model a very different context. For one thing, our $\sum_s E_{pot}$ is a physiologically defined maximum transpiration (not including soil evaporation) for a

particular stand water conducting capacity and growing season rather than the meteorologically based reference PET. For another, we are modeling single growing seasons at the stand scale rather than long-term equilibration of catchment water balance. However, this physiologically based approach does provide a roadmap to accurately infer the role of hydrology in stand function, and incorporate the dynamics of tree mortality and stomatal regulation. This advancement could facilitate upscaling forecasts of patch scale hydrology to watershed and regional dynamics under climate change (Thompson et al., 2011). Bridging the gap between short-term stand and long-term catchment would require linking physiologically based vegetation models to a 3-D hydrological model (e.g., PARFLOW; Tai et al., 2018) at a landscape scale. Such an approach would constrain the mechanisms by which any root zone subsidy could be realized, including its dependence on winter precipitation regime, and the effects of slope and aspect on water availability and runoff (Zapata-Rios et al., 2016).

The dependency of montane aspen on groundwater subsidy revealed by this study is cause for concern given climate change projections for the intermountain region of the United States: The area is expected to receive less precipitation as snow in the future, and a faster rate of snowpack melt due to rising winter and spring temperatures, as well as dust deposition (Cayan et al., 2013; Deems et al., 2013). Both of these factors may result in less effective recharge of groundwater from winter inputs (Deems et al., 2013; Udall, 2013). Based on the results from this study any reduction in root zone subsidy would be expected to drought-stress many aspen stands and increase their mortality risk. The approach presented in this study provides a framework to develop more robust predictions of forest responses to climate change, which are needed to anticipate effects on forest resources and to inform mitigation by appropriate management practices (Bradford & Bell, 2017).

References

Adams, D. K., & Comrie, A. C. (1997). The North American monsoon. *Bulletin of the American Meteorological Society*, *78*(10), 2197–2213. https://doi.org/10.1175/1520-0477(1997)078<2197:TNAM>2.0.CO;2

Adams, H. D., Zeppel, M. J., Anderegg, W. R., Hartmann, H., Landhäusser, S. M., Tissue, D. T., Huxman, T. E., et al. (2017). A multi-species synthesis of physiological mechanisms in drought-induced tree mortality. *Nature ecology & evolution*, *1*(9), 1285–1291. https://doi.org/10.1038/s41559-017-0248-x

Alder, N. N., Pockman, W. T., Sperry, J. S., & Nuismer, S. (1997). Use of centrifugal force in the study of xylem cavitation. *Journal of Experimental Botany*, *48*(3), 665–674. https://doi.org/10.1093/jxb/48.3.665

Allen, C., Macalady, A., Chenchouni, H., Bachelet, D., McDowell, N., Vennetier, M., Kitzberger, T., et al. (2010). A global overview of drought and heat-induced tree mortality reveals emerging climate change risks for forests. *Forest Ecology and Management*, *259*(4), 660–684. https://doi.org/10.1016/j.foreco.2009.09.001

Anderegg, L. D. L., Anderegg, W. R. L., Abatzoglau, J., Hausladen, A. M., & Berry, J. A. (2013). Drought characteristics' role in widespread aspen forest mortality across Colorado, USA. *Global Change Biology*, *19*(5), 1526–1537. https://doi.org/10.1111/gcb.12146

Anderegg, W. R., Wolf, A., Arango-Velez, A., Choat, B., Chmura, D. J., Jansen, S., Kolb, T., et al. (2018). Woody plants optimise stomatal behaviour relative to hydraulic risk. *Ecology Letters*, *21*(7), 968–977. https://doi.org/10.1111/ele.12962

Anderegg, W. R. L., Berry, J. A., Smith, D. D., Sperry, J. S., Anderegg, L. D. L., & Field, C. B. (2012). The roles of hydraulic and carbon stress in a widespread climate-induced forest die-off. *Proceedings of the National Academy of Sciences of the United States of America*, *109*(1), 233–237. https://doi.org/10.1073/pnas.1107891109

Barbeta, A., & Peñuelas, J. (2017). Relative contribution of groundwater to plant transpiration estimated with stable isotopes. *Scientific Reports*, *7*(1), 10,580. https://doi.org/10.1038/s41598-017-09643-x

Barnett, T. P., Pierce, D. W., Hidalgo, H. G., Bonfils, C., Santer, B. D., Das, T., Bala, G., et al. (2008). Human-induced changes in the hydrology of the western United States. *Science*, *319*(5866), 1080–1083. https://doi.org/10.1126/science.1152538

Bigler, C., Gavin, D. G., Gunning, C., & Veblen, T. T. (2007). Drought induces lagged tree mortality in a subalpine forest in the Rocky Mountains. *Oikos*, *116*(12), 1983–1994. https://doi.org/10.1111/j.2007.0030-1299.16034.x

Bradford, J. B., & Bell, D. M. (2017). A window of opportunity for climate-change adaptation: Easing tree mortality by reducing forest basal area. *Frontiers in Ecology and the Environment*, *15*(1), 11–17. https://doi.org/10.1002/fee.1445

Brodribb, T. J., & Cochard, H. (2009). Hydraulic failure defines the recovery and point of death in water-stressed conifers. *Plant Physiology*, *149*(1), 575–584. https://doi.org/10.1104/pp.108.129783

Bunn, A. G. (2010). Statistical and visual crossdating in R using the dplR library. *Dendrochronologia*, *28*(4), 251–258. https://doi.org/10.1016/j.dendro.2009.12.001

Cabon, A., Martínez-Vilalta, J., Martínez de Aragón, J., Poyatos, R., & De Cáceres, M. (2018). Applying the eco-hydrological equilibrium hypothesis to model root distribution in water-limited forests. *Ecohydrology*, *11*(7), e2015. https://doi.org/10.1002/eco.2015

Campbell, G. S. (1985). *Soil physics with BASIC: Transport models for soil-plant systems* (Vol. 14). Amsterdam: Elsevier.

Campbell, G. S., & Norman, J. N. (1998). *An introduction to environmental biophysics* (2nd ed.). New York: Springer.

Castle, S. L., Thomas, B. F., Reager, J. T., Rodell, M., Swenson, S. C., & Famiglietti, J. S. (2014). Groundwater depletion during drought threatens future water security of the Colorado River basin. *Geophysical Research Letters*, *41*, 5904–5911. https://doi.org/10.1002/2014GL061055

Cayan, D. R., Tyree, M., Kunkel, K. E., Castro, C., Gershunov, A., Barsugli, J., Ray, A. J., et al. (2013). Future climate: Projected average. In *Assessment of climate change in the Southwest United States* (pp. 101–125). Washington, DC: Springer.

Choat, B., Jansen, S., Brodribb, T. J., Cochard, H., Bhaskar, R., Bucci, S. J., Feild, T. S., et al. (2012). Global convergence in the vulnerability of forests to drought. *Nature*, *491*(7426), 752–755. https://doi.org/10.1038/nature11688

Dai, A. (2013). Increasing drought under global warming in observations and models. *Nature Climate Change*, *3*(1), 52–58. https://doi.org/10.1038/NCLIMATE1633

Deems, J. S., Painter, T. H., Barsugli, J. J., Belnap, J., & Udall, B. (2013). Combined impacts of current and future dust deposition and regional warming on Colorado River Basin snow dynamics and hydrology. *Hydrology and Earth System Sciences*, *17*(11), 4401–4413. https://doi.org/10.5194/hess-17-4401-2013

Eagleson, P. S. (1982). Ecological optimality in water-limited natural soil-vegetation systems: 1. Theory and hypothesis. *Water Resources Research*, *18*(2), 325–340. https://doi.org/10.1029/WR018i002p00325

Ehleringer, J. R., & Dawson, T. E. (1992). Water uptake by plants: Perspectives from stable isotope composition. *Plant, Cell & Environment*, *15*(9), 1073–1082. https://doi.org/10.1111/j.1365-3040.1992.tb01657.x

Fan, Y. (2015). Groundwater in the Earth's critical zone: Relevance to large-scale patterns and processes. *Water Resources Research*, *51*, 3052–3069. https://doi.org/10.1002/2015WR017037

Fan, Y., Miguez-Macho, G., Jobbágy, E. G., Jackson, R. B., & Otero-Casal, C. (2017). Hydrologic regulation of plant rooting depth. *Proceedings of the National Academy of Sciences of the United States of America*, *114*(40), 10,572–10,577. https://doi.org/10.1073/pnas.1712381114

Frazer, G., Canham, C., & Lertzman, K. (1999). *Gap light analyzer (GLA): Imaging software to extract canopy structure and gap light transmission indices from true-colour fisheye photographs. Users manual and program documentation, version 2.0.* Millbrook, New York: Simon Fraser University, Burnaby, British Columbia, and the Institute of Ecosystem Studies.

Fritts, H. C. (1974). Relationships of ring widths in arid-site conifers to variations in monthly temperature and precipitation. *Ecological Monographs*, *44*(4), 411–440. https://doi.org/10.2307/1942448

Fu, Y. H., Campioli, M., Deckmyn, G., & Janssens, I. A. (2012). The impact of winter and spring temperatures on temperate tree budburst dates: Results from an experimental climate manipulation. *PLoS One*, *7*(10), e47324. https://doi.org/10.1371/journal.pone.0047324

Garreaud, R. D., Alvarez-Garreton, C., Barichivich, J., Boisier, J. P., Duncan, C., Galleguillos, M., LeQuesne, C., et al. (2017). The 2010–2015 megadrought in central Chile: Impacts on regional hydroclimate and vegetation. *Hydrology and Earth System Sciences*, *21*(12), 6307–6327. https://doi.org/10.5194/hess-21-6307-2017

Gifford, G. F. (1966). Aspen root studies on three sites in northern Utah. *American Midland Naturalist*, *75*(1), 132–141. https://doi.org/10.2307/2423485

Hanson, P. J., & Weltzin, J. F. (2000). Drought disturbance from climate change: Response of United States forests. *Science of the Total Environment*, *262*(3), 205–220. https://doi.org/10.1016/S0048-9697(00)00523-4

Holmes, R. L. (1983). Computer-assisted quality control in tree-ring dating and measurement. *Tree-Ring Bulletin*, *43*, 69–78.

Horel, J., Splitt, M., Dunn, L., Pechmann, J., White, B., Ciliberti, C., Lazarus, S., et al. (2002). Mesowest: Cooperative mesonets in the western United States. *Bulletin of the American Meteorological Society*, *83*(2), 211–225. https://doi.org/10.1175/1520-0477(2002)083<0211:MCMITW>2.3.CO;2

Hu, J., Moore, D. J., Burns, S. P., & Monson, R. K. (2010). Longer growing seasons lead to less carbon sequestration by a subalpine forest. *Global Change Biology*, *16*(2), 771–783. https://doi.org/10.1111/j.1365-2486.2009.01967.x

Jacobsen, A. L., Pratt, R. B., Davis, S. D., & Tobin, M. F. (2014). Geographic and seasonal variation in chaparral vulnerability to cavitation. *Madrono*, *61*(4), 317–327. https://doi.org/10.3120/0024-9637-61.4.317

Keppel, G., Van Niel, K. P., Wardell-Johnson, G. W., Yates, C. J., Byrne, M., Mucina, L., Schut, A. G. T., et al. (2012). Refugia: Identifying and understanding safe havens for biodiversity under climate change. *Global Ecology and Biogeography*, *21*(4), 393–404. https://doi.org/10.1111/j.1466-8238.2011.00686.x

Kolb, K. J., & Sperry, J. S. (1999). Differences in drought adaptation between subspecies of sagebrush (*Artemisia tridentata*). *Ecology*, *80*(7), 2373–2384. https://doi.org/10.1890/0012-9658(1999)080[2373:DIDABS]2.0.CO;2.

Litvak, E., McCarthy, H. R., & Pataki, D. E. (2012). Transpiration sensitivity of urban trees in a semi-arid climate is constrained by xylem vulnerability to cavitation. *Tree Physiology*, *32*(4), 373–388. https://doi.org/10.1093/treephys/tps015

Lopez, O. R., Kursar, T. A., Cochard, H., & Tyree, M. T. (2005). Interspecific variation in xylem vulnerability to cavitation among tropical tree and shrub species. *Tree Physiology*, *25*(12), 1553–1562. https://doi.org/10.1093/treephys/25.12.1553

López, R., Cano, F. J., Choat, B., Cochard, H., & Gil, L. (2016). Plasticity in vulnerability to cavitation of *Pinus canariensis* occurs only at the driest end of an aridity gradient. *Frontiers in Plant Science*, *7*, 769. https://doi.org/10.3389/fpls.2016.00769

López, R., de Heredia, U. L., Collada, C., Cano, F. J., Emerson, B. C., Cochard, H., & Gil, L. (2013). Vulnerability to cavitation, hydraulic efficiency, growth and survival in an insular pine (*Pinus canariensis*). *Annals of Botany*, *111*(6), 1167–1179. https://doi.org/10.1093/aob/mct084

Mackay, D. S., Roberts, D. E., Ewers, B. E., Sperry, J. S., McDowell, N., & Pockman, W. (2015). Interdependence of chronic hydraulic dysfunction and canopy processes can improve integrated models of tree response to drought. *Water Resources Research*, *51*, 6156–6176. https://doi.org/10.1002/2015WR017244

Maherali, H., Pockman, W. T., & Jackson, R. B. (2004). Adaptive variation in the vulnerability of woody plants to xylem cavitation. *Ecology*, *85*(8), 2184–2199. https://doi.org/10.1890/02-0538

Martin, J. G., Kloeppel, B. D., Schaefer, T. L., Kimbler, D. L., & McNulty, S. G. (1998). Aboveground biomass and nitrogen allocation of ten deciduous southern Appalachian tree species. *Canadian Journal of Forest Research*, *28*(11), 1648–1659. https://doi.org/10.1139/cjfr-28-11-1648

Maurer, G. E., & Bowling, D. R. (2014). Seasonal snowpack characteristics influence soil temperature and water content at multiple scales in interior western US mountain ecosystems. *Water Resources Research*, *50*, 5216–5234. https://doi.org/10.1002/2013WR014452

McDowell, N., Fisher, R. A., Xu, C., Domec, J. C., Holtta, T., Mackay, D. S., Sperry, J. S., et al. (2013). Evaluating theories of drought-induced vegetation mortality using a multimodel-experimental framework. *New Phytologist*, *200*(2), 304–321. https://doi.org/10.1111/nph.12465.

McDowell, N., Pockman, W. T., Allen, C. D., Breshears, D. D., Cobb, N., Kolb, T., Plaut, J., et al. (2008). Mechanisms of plant survival and mortality during drought. Why do some plants survive while others succumb to drought? *New Phytologist*, *178*(4), 719–739. https://doi.org/10.1111/j.1469-8137.2008.02436.x.

McLaughlin, B. C., Ackerly, D. D., Klos, P. Z., Natali, J., Dawson, T. E., & Thompson, S. E. (2017). Hydrologic refugia, plants, and climate change. *Global Change Biology*, *23*(8), 2941–2961. https://doi.org/10.1111/gcb.13629

Medlyn, B. E., Dreyer, E., Ellsworth, D. S., Forstreuter, M., Harley, P. C., Kirschbaum, M. U. F., Le Roux, X., et al. (2002). Temperature response of parameters of a biochemically based model of photosynthesis. II. A review of experimental data. *Plant, Cell & Environment*, *25*(9), 1167–1179. https://doi.org/10.1046/j.1365-3040.2002.00891.x

Miguez-Macho, G., & Fan, Y. (2012). The role of groundwater in the Amazon water cycle: 2. Influence on seasonal soil moisture and evapotranspiration. *Journal of Geophysical Research*, *117*, D15114. https://doi.org/10.1029/2012JD017540

Naumburg, E., Mata-Gonzalez, R., Hunter, R. G., Mclendon, T., & Martin, D. W. (2005). Phreatophytic vegetation and groundwater fluctuations: A review of current research and application of ecosystem response modeling with an emphasis on Great Basin vegetation. *Environmental Management*, *35*(6), 726–740. https://doi.org/10.1007/s00267-004-0194-7

Newman, B. D., Wilcox, B. P., Archer, S. R., Breshears, D. D., Dahm, C. N., Duffy, C. J., McDowell, N. G., et al. (2006). Ecohydrology of water-limited environments: A scientific vision. *Water Resources Research*, *42*, W06302. https://doi.org/10.1029/2005WR004141

Pockman, W. T., & Sperry, J. S. (2000). Vulnerability to cavitation and the distribution of Sonoran desert vegetation. *American Journal of Botany*, *87*(9), 1287–1299. https://doi.org/10.2307/2656722

Powell, T., Galbraith, D., Christoffersen, B., Harper, A., Imbuzeiro, H., Rowland, L., Almeida, S., et al. (2013). Confronting model predictions of carbon fluxes with measurements of Amazon forests subjected to experimental drought. *New Phytologist*, *200*(2), 350–365. https://doi.org/10.1111/nph.12390

R Core Team (2016). *R: A language and environment for statistical computing*. Vienna, Austria: R Foundation for Statistical Computing. Retrieved from https://www.R-project.org/

Richter, D. d., & Billings, S. A. (2015). 'One physical system': Tansley's ecosystem as Earth's critical zone. *New Phytologist*, *206*(3), 900–912. https://doi.org/10.1111/nph.13338

Rodríguez-Calcerrada, J., Li, M., López, R., Cano, F. J., Oleksyn, J., Atkin, O. K., Pita, P., et al. (2017). Drought-induced shoot dieback starts with massive root xylem embolism and variable depletion of nonstructural carbohydrates in seedlings of two tree species. *New Phytologist*, *213*(2), 597–610. https://doi.org/10.1111/nph.14150

Sack, L., & Tyree, M. T. (2005). Leaf hydraulics and its implications in plant structure and function. In N. M. Holbrook & M. A. Zwieniecki (Eds.), *Vascular transport in plants* (pp. 93–114). Oxford: Elsevier/Academic Press. https://doi.org/10.1016/B978-012088457-5/50007-1

Snyder, K. A., & Williams, D. G. (2000). Water sources used by riparian trees varies among stream types on the San Pedro River, Arizona. *Agricultural and Forest Meteorology*, *105*(1–3), 227–240. https://doi.org/10.1016/S0168-1923(00)00193-3

Sperry, J. S., Adler, F. R., Campbell, G. S., & Comstock, J. P. (1998). Limitation of plant water use by rhizosphere and xylem conductance: Results from a model. *Plant, Cell & Environment*, *21*(4), 347–359. https://doi.org/10.1046/j.1365-3040.1998.00287.x

Sperry, J. S., Hacke, U. G., Oren, R., & Comstock, J. P. (2002). Water deficits and hydraulic limits to leaf water supply. *Plant, Cell & Environment*, *25*(2), 251–263. https://doi.org/10.1046/j.0016-8025.2001.00799.x

Sperry, J. S., & Love, D. M. (2015). What plant hydraulics can tell us about plant responses to climate-change droughts. *New Phytologist*, *207*(1), 14–27. https://doi.org/10.1111/nph.13354

Sperry, J. S., & Tyree, M. T. (1988). Mechanism of water stress-induced xylem embolism. *Plant Physiology*, *88*(3), 581–587. https://doi.org/10.1104/pp.88.3.581

Sperry, J. S., Venturas, M. D., Anderegg, W. R., Mencuccini, M., Mackay, D. S., Wang, Y., & Love, D. M. (2017). Predicting stomatal responses to the environment from the optimization of photosynthetic gain and hydraulic cost. *Plant, Cell & Environment*, *40*(6), 816–830. https://doi.org/10.1111/pce.12852

Sperry, J. S., Wang, Y., Wolfe, B., Mackay, D. S., Anderegg, W. R. L., McDowell, N. G., & Pockman, W. T. (2016). Pragmatic hydraulic theory predicts stomatal responses to climatic water deficits. *New Phytologist*, *212*(3), 577–589. https://doi.org/10.1111/nph.14059

Stewart, J. R., Lister, A. M., Barnes, I., & Dalén, L. (2010). Refugia revisited: Individualistic responses of species in space and time. *Proceedings of the Royal Society B: Biological Sciences*, *277*(1682), 661–671. https://doi.org/10.1098/rspb.2009.1272

Stokes, M. A., & Smiley, T. L. (1996). *An introduction to tree-ring dating*. Tucson: University of Arizona Press.

Swetnam, T. L., Brooks, P. D., Barnard, H. R., Harpold, A. A., & Gallo, E. L. (2017). Topographically driven differences in energy and water constrain climatic control on forest carbon sequestration. *Ecosphere*, *8*(4). https://doi.org/10.1002/ecs2.1797

Tai, X., Mackay, D. S., Anderegg, W. R., Sperry, J. S., & Brooks, P. D. (2017). Plant hydraulics improves and topography mediates prediction of aspen mortality in southwestern USA. *New Phytologist*, *213*(1), 113–127. https://doi.org/10.1111/nph.14098

Tai, X., Mackay, D. S., Sperry, J. S., Brooks, P. D., Anderegg, W. R. L., Flanagan, L. B., Rood, S. B., et al. (2018). Distributed plant hydraulic and hydrological modeling to understand the susceptibility of riparian woodland trees to drought-induced mortality. *Water Resources Research*, *54*, 4901–4915. https://doi.org/10.1029/2018WR022801

Thompson, S., Harman, C., Troch, P. A., Brooks, P. D., & Sivapalan, M. (2011). Spatial scale dependence of ecohydrologically mediated water balance partitioning: A synthesis framework for catchment ecohydrology. *Water Resources Research*, *47*, W00J03. https://doi.org/10.1029/2010WR009998

Tobin, M. F., Pratt, R. B., Jacobsen, A. L., & De Guzman, M. E. (2013). Xylem vulnerability to cavitation can be accurately characterised in species with long vessels using a centrifuge method. *Plant Biology*, *15*(3), 496–504. https://doi.org/10.1111/j.1438-8677.2012.00678.x

Udall, B. (2013). Water: Impacts, risks, and adaptation. In A. J. G. Garfin, R. Merideth, M. Black, & S. LeRoy (Eds.), *Assessment of climate change in the Southwest United States: A report prepared for the National Climate Assessment* (pp. 197–217). Washington, DC: Island Press. https://doi.org/10.5822/978-1-61091-484-0_10

van Genuchten, M. T. (1980). A closed form equation for predicting the hydraulic conductivity of unsaturated soils. *Soil Science Society of America Journal*, *44*(5), 892–898. https://doi.org/10.2136/sssaj1980.03615995004400050002x

Venturas, M. D., MacKinnon, E. D., Dario, H. L., Jacobsen, A. L., Pratt, R. B., & Davis, S. D. (2016). Chaparral shrub hydraulic traits, size, and life history types relate to species mortality during California's historic drought of 2014. *PLoS One*, *11*(7), e0159145. https://doi.org/10.1371/journal.pone.0159145

Venturas, M. D., Sperry, J. S., Love, D. M., Frehner, E. H., Allred, M. G., Wang, Y., & Anderegg, W. R. (2018). A stomatal control model based on optimization of carbon gain versus hydraulic risk predicts aspen sapling responses to drought. *The New Phytologist*, *220*(3), 836–850. https://doi.org/10.1111/nph.15333

Vinya, R., Malhi, Y., Fisher, J. B., Brown, N., Brodribb, T. J., & Aragao, L. E. (2013). Xylem cavitation vulnerability influences tree species' habitat preferences in miombo woodlands. *Oecologia*, *173*(3), 711–720. https://doi.org/10.1007/s00442-013-2671-2

von Allmen, E. I., Sperry, J. S., & Bush, S. E. (2015). Contrasting whole-tree water use, hydraulics, and growth in a co-dominant diffuse-porous vs. ring-porous species pair. *Trees-Structure and Function*, *29*(3), 717–728. https://doi.org/10.1007/s00468-014-1149-0

Wang, T., Hamann, A., Spittlehouse, D., & Carroll, C. (2016). Locally downscaled and spatially customizable climate data for historical and future periods for North America. *PLoS One*, *11*(6), e0156720. https://doi.org/10.1371/journal.pone.0156720

West, A. G., Dawson, T., February, E., Midgley, G., Bond, W., & Aston, T. (2012). Diverse functional responses to drought in a Mediterranean-type shrubland in South Africa. *New Phytologist*, *195*(2), 396–407. https://doi.org/10.1111/j.1469-8137.2012.04170.x

Williams, A. P., Allen, C. D., Macalady, A. K., Griffin, D., Woodhouse, C. A., Meko, D. M., Swetnam, T. W., et al. (2013). Temperature as a potent driver of regional forest drought stress and tree mortality. *Nature Climate Change*, *3*(3), 292–297. https://doi.org/10.1038/NCLIMATE1693

Wolf, A., Anderegg, W. R. L., & Pacala, S. W. (2016). Optimal stomatal behavior with competition for water and risk of hydraulic impairment. *Proceedings of the National Academy of Sciences of the United States of America*, *113*(46), E7222–E7230. https://doi.org/10.1073/pnas.1615144113

Zang, C., & Biondi, F. (2015). treeclim: An R package for the numerical calibration of proxy-climate relationships. *Ecography*, *38*(4), 431–436. https://doi.org/10.1111/ecog.01335

Zapata-Rios, X., Brooks, P. D., Troch, P. A., McIntosh, J., & Guo, Q. (2016). Influence of terrain aspect on water partitioning, vegetation structure and vegetation greening in high-elevation catchments in northern New Mexico. *Ecohydrology*, *9*(5), 782–795. https://doi.org/10.1002/eco.1674

Zhang, L., Dawes, W., & Walker, G. (2001). Response of mean annual evapotranspiration to vegetation changes at catchment scale. *Water Resources Research*, *37*(3), 701–708. https://doi.org/10.1029/2000WR900325